

Microstructure analysis and thermal stability of Mg²⁺/Sr²⁺/SO₄²⁻ ions doped hydroxyapatite bionanomaterials

A. Z. Alshemary^{a,b,c,*}, Y. Muhammed^c, İ. S. Çardaklı^d, A. B. Marandi^e

^aDepartment of Chemistry, College of Science and Technology, Wenzhou-Kean University, Wenzhou, 325060, China.

^bBiomedical Engineering Department, Al-Mustaqbal University College, Hillah, Babil 51001, Iraq.

^cAeronautical Techniques Engineering, AL-Farahidi University, Baghdad, Iraq.

^dDepartment of Metallurgical and Materials Engineering, Atatürk University, Erzurum, 25240, Turkey

^eBiomedical Engineering Department, Faculty of Engineering, Karabuk University, Karabuk, 78050, Turkey

This study evaluates the influence of the addition of Mg²⁺, Sr²⁺, and SO₄²⁻ ions on the microstructure and thermal stability of hydroxyapatite (HA). The materials were calcined at 500 °C and 800 °C for 2 h, then characterized by XRD, FTIR, SEM, EDX, and FTIR techniques. The degree of crystallinity and crystallite size of HA crystals were significantly decreased with the incorporation of Mg²⁺/Sr²⁺/SO₄²⁻ ions. While the lattice parameters were reduced due to the substitution of ions, The high incorporation of Mg²⁺ ions lowered the thermal stability of HA. At the same time, the addition of Sr²⁺ ions enhanced thermal stability. A similar impact on phosphate bands was seen in FTIR results. HA existed in spherical nanoparticles; incorporating Mg, Sr, and S ions doesn't change the particle shape.

(Received October 4, 2022; Accepted January 4, 2023)

Keywords: Hydroxyapatite, Substitution, XRD, FTIR, Thermal stability

1. Introduction

With its high biocompatibility and high bioactivity, hydroxyapatite (HA) is a sophisticated ceramic material that has been widely used in the medical field. Because of its exceptional biocompatibility and bioactivity, HA is one of the sophisticated ceramic materials widely recognized in biomedical applications. Several scientific studies might benefit from its bioactive characteristics, which makes it a possible source for a substantial number of research inquiries. Consequently, it has numerous applications in diverse fields such as biomedical, chromatography, water purification, and catalysis. It can not only integrate into bone structures but at the same time also supports bone growth. This property makes HA attractive and widely used as a bone implant material. Biological apatite is significantly different from its synthetic counterpart HA. The main differences are in terms of structure, composition, crystallinity, solubility, biological activity, ability to promote bone formation, and other physical and mechanical properties. There is clear evidence that the inferiority of HA to biological apatite is due to the absence of essential inorganic ions found in biological apatite. To overcome this deficiency, researchers have focused their attention on improving the biological properties of HA by incorporating beneficial ions such as Zn⁺² [1], K⁺¹ [2], SO₄²⁻ [3], etc., which were present in the inorganic part of the mammalian hard tissue.

These ions can play a vital role in improving the biological activity of synthetic apatite. The significance of these ions has provoked scientists to prepare substituted HA to mimic biological apatite, this similarity in turn, enhances osteointegration and bioactivity of HA [4, 5]. The properties of the substituted apatite will be determined by the ion included, the quantity of doping, and the substitution location. These ions may act as a replacement for calcium, phosphate,

* Corresponding author: aalshema@kean.edu
<https://doi.org/10.15251/DJNB.2023.181.1>

or the hydroxyl group. These replacements may be performed separately on a single ion or concurrently on many ions.

HA is substituted with trace amounts of certain ions like Magnesium (Mg^{2+}), Strontium (Sr^{2+}), and Sulphate (SO_4^{2-}) metabolic processes of living organisms. For example, low doses of Sr^{2+} ion significantly affected osteoporosis therapy [6]. It has been proven to help reduce fracture incidence in osteoporotic patients [7, 8]. Similarly, a small amount of Mg^{2+} ion, like insulin, directly stimulates osteoblast proliferation (an identified growth factor for osteoblast) [9]. Similarly, SO_4^{2-} ion has the capability to affect the catabolic and anabolic processes of skin cells, hair, nails, and cartilage and protects cartilage from osteoarthritis [10, 11]. Tri-ion substituted HA still has less attention from the researcher. This research aims to synthesize the monophasic Mg^{2+} , Sr^{2+} , and SO_4^{2-} doped hydroxyapatite nano powders with good crystallinity.

2. Experimental

The required chemicals were purchased from (Qrec, Newzeland) and used without further purification. Different series of HA substituted with Mg^{2+} , Sr^{2+} and SO_4^{2-} (Table 1) were synthesized using microwave-assisted precipitation.

Calcium nitrate, magnesium nitrate and strontium nitrate were dissolved in 100ml of double-distilled water. Di-ammonium hydrogen phosphate and sodium sulphate were dissolved in 100ml of double-distilled water, the last one was added dropwise under magnetic stirring, adjusting pH >10 using ammonium hydroxide and refluxed under microwave irradiations (SHARP, model R-218LS) at 800 W, for 30 mins exposure time. The HA was collected, filtered, washed and dried at 80°C for 17 hrs. All samples were heated-treated at 500°C and 800 °C for 2h.

Table 1. Amount of reactant added

| Sample ID | Reactant (mole) | | | | |
|-----------|-----------------|------|------|-----------------|-----------------|
| | Ca | Mg | Sr | PO ₄ | SO ₄ |
| HA | 1.0 | 0.00 | 0.00 | 0.60 | 0.00 |
| 1Mg-SHA | 0.9 | 0.01 | 0.00 | 0.55 | 0.05 |
| 2MgSr-SHA | 0.9 | 0.08 | 0.02 | 0.55 | 0.05 |
| 3MgSr-SHA | 0.9 | 0.06 | 0.04 | 0.55 | 0.05 |
| 4MgSr-SHA | 0.9 | 0.04 | 0.06 | 0.55 | 0.05 |
| 5MgSr-SHA | 0.9 | 0.02 | 0.08 | 0.55 | 0.05 |
| 6Sr-SHA | 0.9 | 0.00 | 0.10 | 0.55 | 0.05 |

Patterns from the Bruker D8 Advance XRD diffractometer, which was operated at 40 kV and 40mA with Cu K radiation at a step size of 0.02° and step duration of 1sec, revealed the phase purity of HA and MgSr-SHA series, respectively. The Jade 6.5 software was used to figure out the lattice parameters, degree of crystallinity, crystallite size, and the ratio of phases [12]. FTIR Bruker (optic GmbH) ALPHA-T was used to identify functional groups using the traditional KBr pellet approach, 16 scans collected spectra in the 400–4000 cm⁻¹ range. The morphology of particles and Ca/P ratio were evaluated using CARL ZEISS ULTRA PLUS GEMINI FESEM. To investigate the manufactured materials' resistance to heat, a thermogravimetric analysis (TGA, PerkinElmer Pyris 1) was performed in a nitrogen environment from ambient temperature to 950 °C, during which the weights of the samples were continuously recorded.

The practical steps, including the preparation and characterization of MgSr-SHA, as a flowchart, are presented in Figure 1.

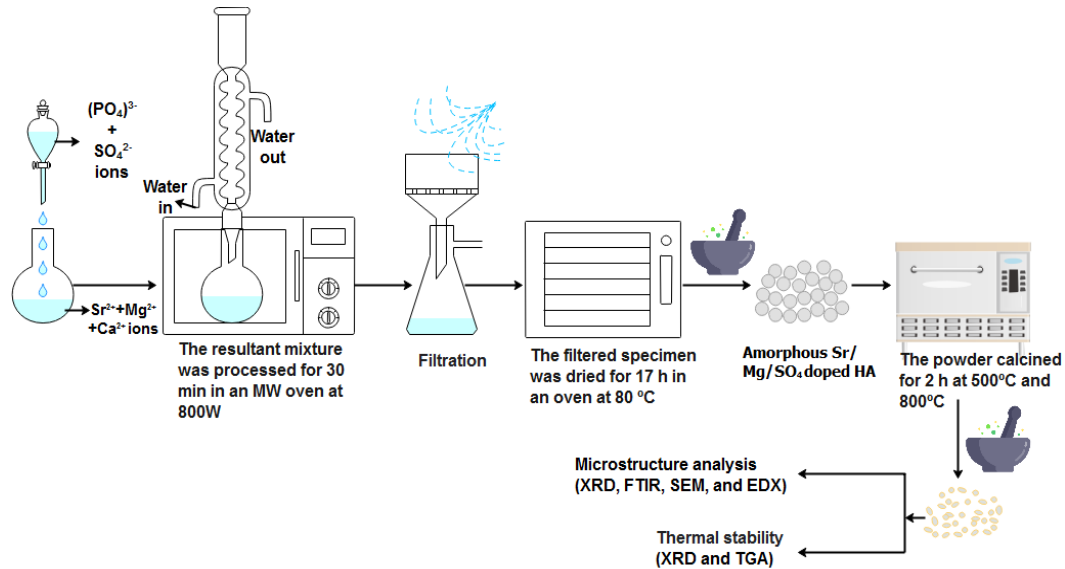
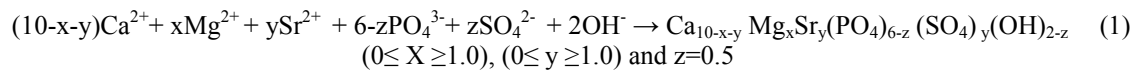


Fig. 1. Experiment flow chart.

3. Results and discussions

Different series of HA substituted with Mg²⁺, Sr²⁺ and SO₄²⁻ (**Table 1**) were synthesized using microwave-assisted precipitation following the reaction expressed in Equation (1).



The XRD patterns of the prepared materials calcined at 800 °C are illustrated in Figure 2. The diffraction planes of HA were in good match with the standard phase of pure HA (JCDPS 09-432), indicating that pure HA is thermally stable at 800 °C. However, the XRD pattern 1Mg-SHA revealed that high incorporation amount of Mg²⁺ ions reduced the thermal stability of HA. The HA phase was partially decomposed to βTricalcium phosphate (βTCP, JCPDS 09-0169). The ratio of βTCP gradually increased upon increasing the incorporation amount of Mg²⁺ ions (Figure 3), confirming that the Mg²⁺ ions destabilize the HA crystal structure to furnish thermally unstable MgSr-SHA [13]. However, with increasing the Sr/Ca+Mg ratio in the adopted synthesis enhanced the thermal instability of materials. It was observed that even a little quantity of Sr (0.02 mol) stabilizes the HA phase and decreases the amount of TCP from 6.19% to 5.20%, with the impact seeming to be stronger in the case of the lowest concentration.

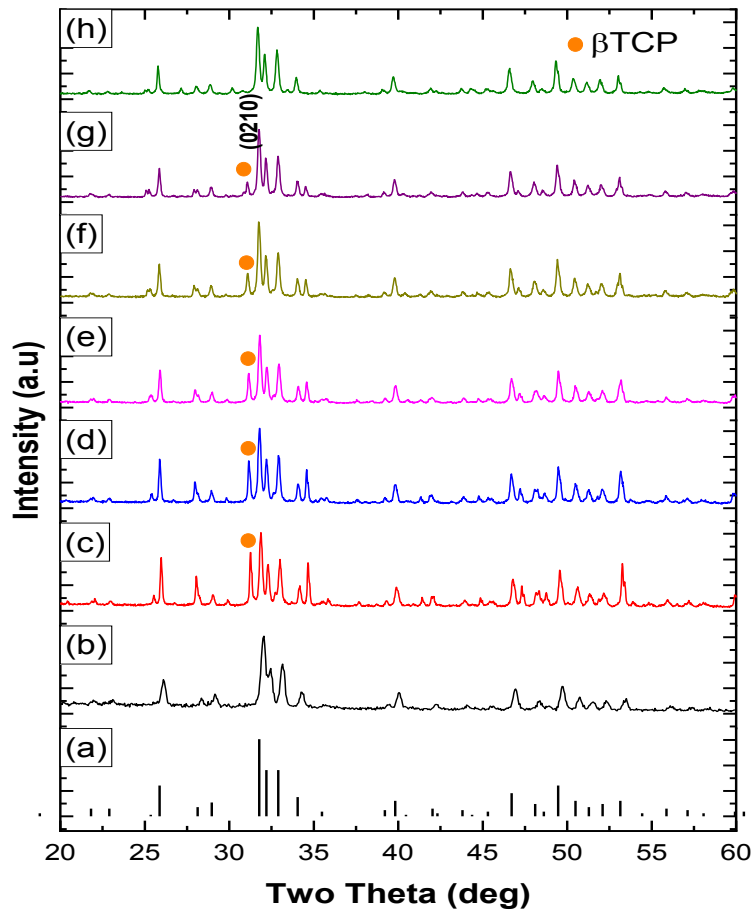


Fig. 2. XRD pattern of (a) standard HA (JCDPS NO:09-432), (b) pure HA, (c) 1Mg-SHA, (d) 2MgSr-SHA, (e) 3MgSr-SHA, (f) 4MgSr-SHA, (g) 5MgSr-SHA, and (h) 6Sr-SHA calcined at 800 °C.

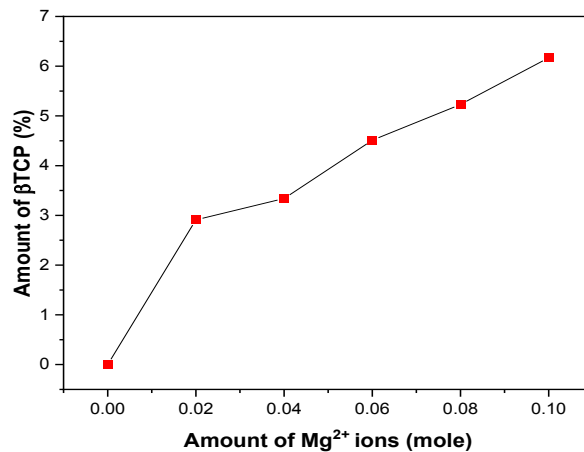


Fig. 3. Amount of βTCP phase.

In order to investigate the thermal characteristics of the materials, TGA testing was carried out (Fig. 4). The TGA curves of the crystals exhibit three clearly defined regions. At temperatures between 700 and 800 °C, HA may break down into two-phase materials, HA and TCP. Lattice water is evaporated at temperatures between 90 and 150 °C, whereas absorbed water from sample surfaces is eliminated between 45 and 90 °C. The percentages of total weight loss for pure HA, 1Mg-SHA, 4MgSr-SHA, and 1Sr-SHA, respectively, were 21.39%, 20.21%, 28.64%, 13.90%, and

9.89%. Because it had the largest ratio of Sr ions compared to the others, the 1Sr-SHA material exhibited the greatest degree of thermal stability.

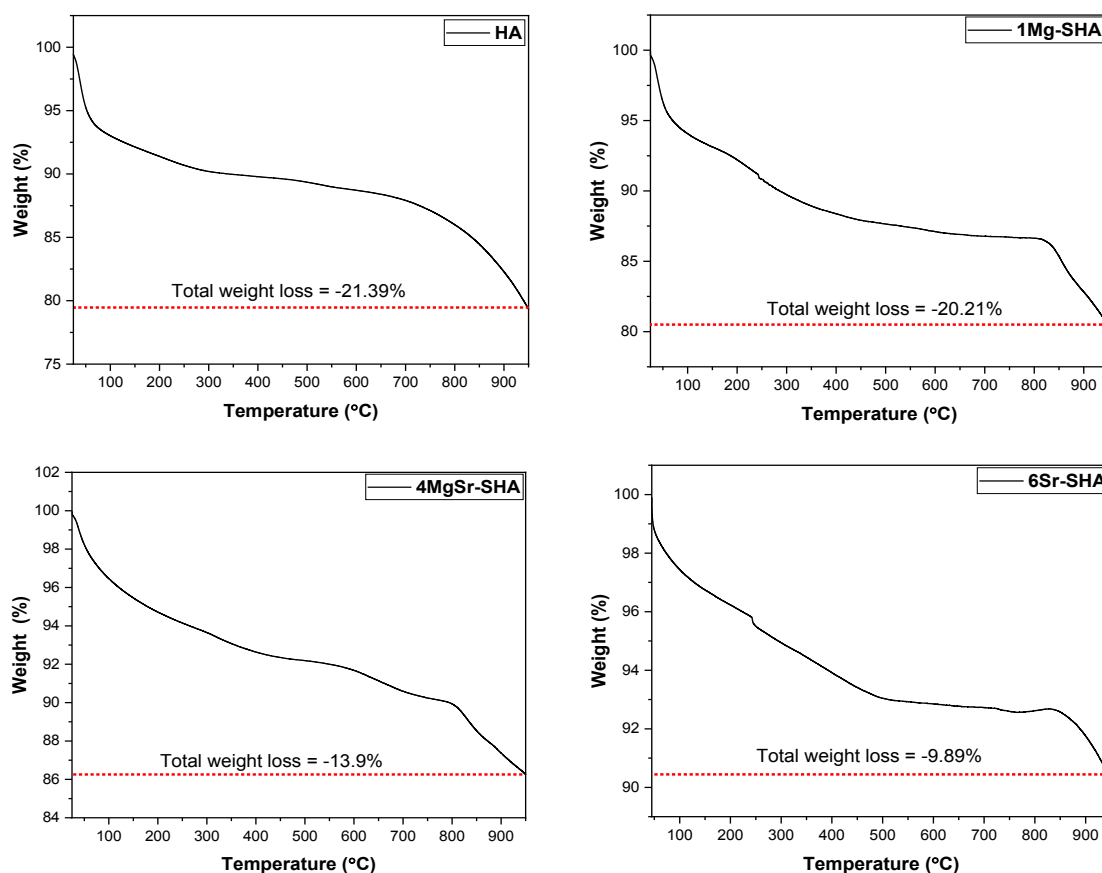


Fig. 4. TGA analysis of the prepared materials.

Figure 4 shows XRD analysis of the calcined HA and MgSr-SHA series, confirming the formation of phase pure crystalline HA (JCPDS # 09-0432). Additional phase-related peaks: tricalcium phosphate and calcium oxide were not observed. Results showed that incorporating Mg^{2+} and Sr^{2+} ions into SHA led to shifting the diffraction peaks toward lower diffraction angles. This result is in good agreement with our previous result that the incorporation of sulphate in HA showed an increase in lattice parameter and shifted towards a lower 2 theta value due to the larger ionic radius of SO_4^{2-} (0.258 nm) compared to PO_4^{3-} (0.238 nm). However, in this dataset, the shifting in the XRD peaks is in the reverse direction (towards higher 2 theta value) with an increasing amount of Sr^{2+} ions in the Mg-SHA lattice, whereas a clear reduction in peak intensity and an increased peak broadening could be observed from the XRD peaks. This could be attributed to the loss of crystallinity and a reduction in the crystalline size. In the same way, changes in the textural parameters could be caused by differences in ionic radius. This is because Ca^{2+} ions (0.099 nm) are replaced by smaller Mg^{2+} ions (0.065 nm) and bigger Sr^{2+} ions (0.120 nm). We think that swapping larger ions for smaller ones changes the shape of the HA lattice (Table 2).

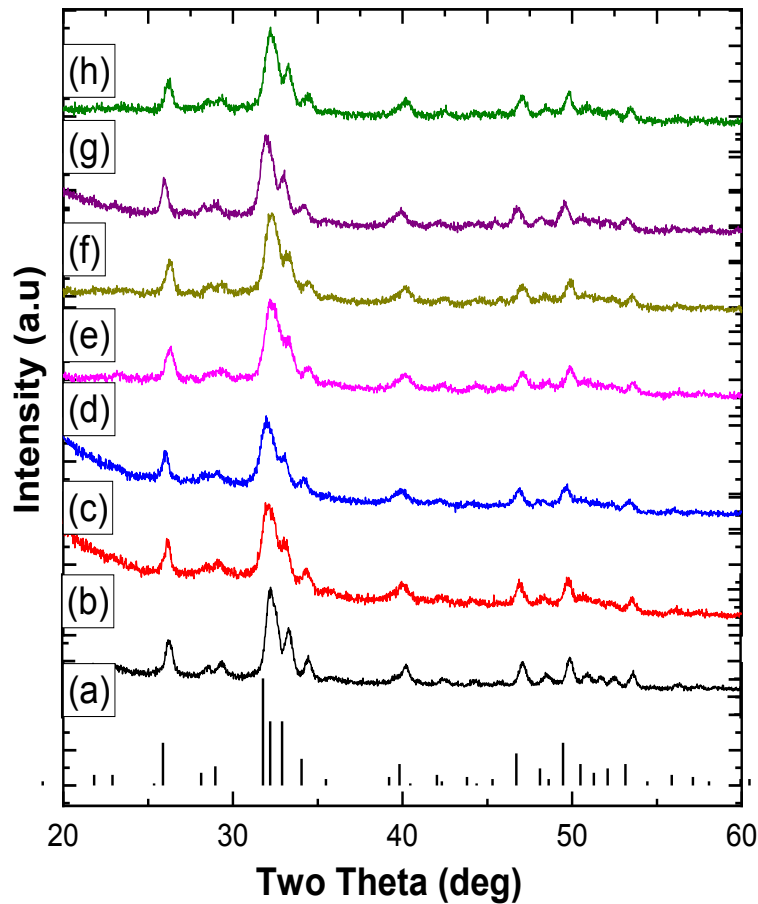


Fig. 4. XRD pattern of (a) standard HA (JCDPS NO:09-432), (b) pure HA, (c) 1Mg-SHA, (d) 2MgSr-SHA, (e) 3MgSr-SHA, (f) 4MgSr-SHA, (g) 5MgSr-SHA, and (h) 6Sr-SHA calcined at 500 °C.

Table 2. Lattice parameters, crystallite size and degree of crystallinity of pure ha and MgSr-SHA series.

| Sample ID | Lattice Parameters | | | Crystallite size (nm) | Degree of Crystallinity (%) |
|-----------|--------------------|------------|---------------------------|-----------------------|-----------------------------|
| | a-Axis (Å) | c-Axis (Å) | Cell Vol (Å) ³ | | |
| HA | 9.428 | 6.805 | 523 | 70 | 40 |
| 1Mg-SHA | 9.391 | 6.839 | 522 | 61 | 36 |
| 2MgSr-SHA | 9.347 | 6.860 | 519 | 62 | 33 |
| 3MgSr-SHA | 9.396 | 6.823 | 521 | 64 | 31 |
| 4MgSr-SHA | 9.384 | 6.838 | 521 | 58 | 29 |
| 5MgSr-SHA | 9.396 | 6.864 | 524 | 59 | 30 |
| 6Sr-SHA | 9.442 | 6.824 | 527 | 56 | 33 |

FTIR analysis is shown in Figure 4, where the sulphate-induced changes in the bands of HA can be noticed. In terms of stretching and vibration, the O-H group may be divided into two bands: 3577 cm⁻¹ and 632 cm⁻¹. An absorption spectrum showed that the phosphate group was responsible for four distinct absorption bands. Examples include the O-P-O vibrational mode at 473 cm⁻¹ and the O-P-O bending mode peaks at 565 cm⁻¹ and 602 cm⁻¹. One O-H water bending vibration mode, with a wavelength of 1643cm⁻¹, was detected in the FTIR spectrum [14].

The absence of a peak at 867 cm⁻¹ (HPO₄⁻) in all samples confirmed the phase purity of HA. FTIR results agree with XRD results (Figure 3) as the spectral peaks become broad and show a reduction in their intensity due to the substitution of Mg²⁺, Sr²⁺ and SO₄⁻² ions. Figure. 4 shows

the disappearance of OH bending at 632 cm^{-1} in the SHA series, which could be the effect of replacing the OH⁻ group with SO_4^{2-} ions to balance the charge on the HA surface.

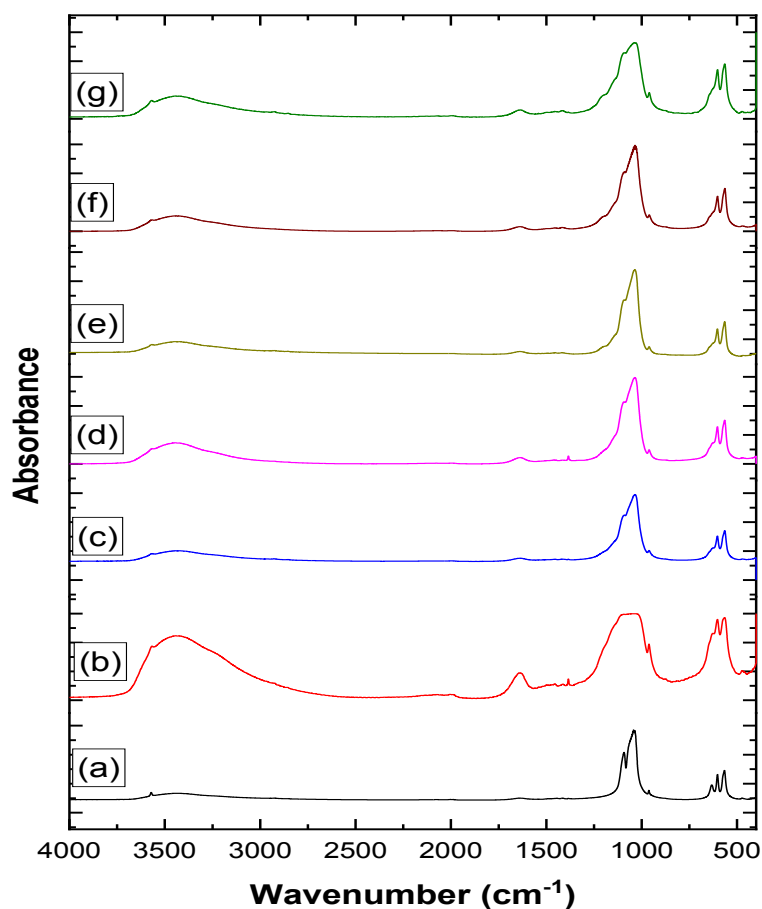


Fig. 5. FTIR spectra of (a) pure HA, (b) 1Mg-SHA, (c) 2MgSr-SHA, (d) 3MgSr-SHA, (e) 4MgSr-SHA, (f) 5MgSr-SHA, and (g) 6Sr-SHA calcined at 500 °C.

Fig. 5 displays FESEM micrographs of MgSr-SHA materials. The synthesized components seemed to be uniformly and randomly dispersed into spherical forms, each having its own unique aggregation and connectivity structure. The dispersion of the HA nanoparticles was even, and their form was spherical. Co-substitution of Mg^{2+} and Sr^{2+} ions resulted in substantial alterations in the aggregation state and interfacial interaction of the HA nanoparticles. Based on the EDX results, all nanoparticles had a substantial amount of the elements Ca and P. Subsequent elemental analysis of the MgSr-SHA nanoparticles provided additional evidence that the Mg/Sr/S ions had been effectively integrated into the HA.

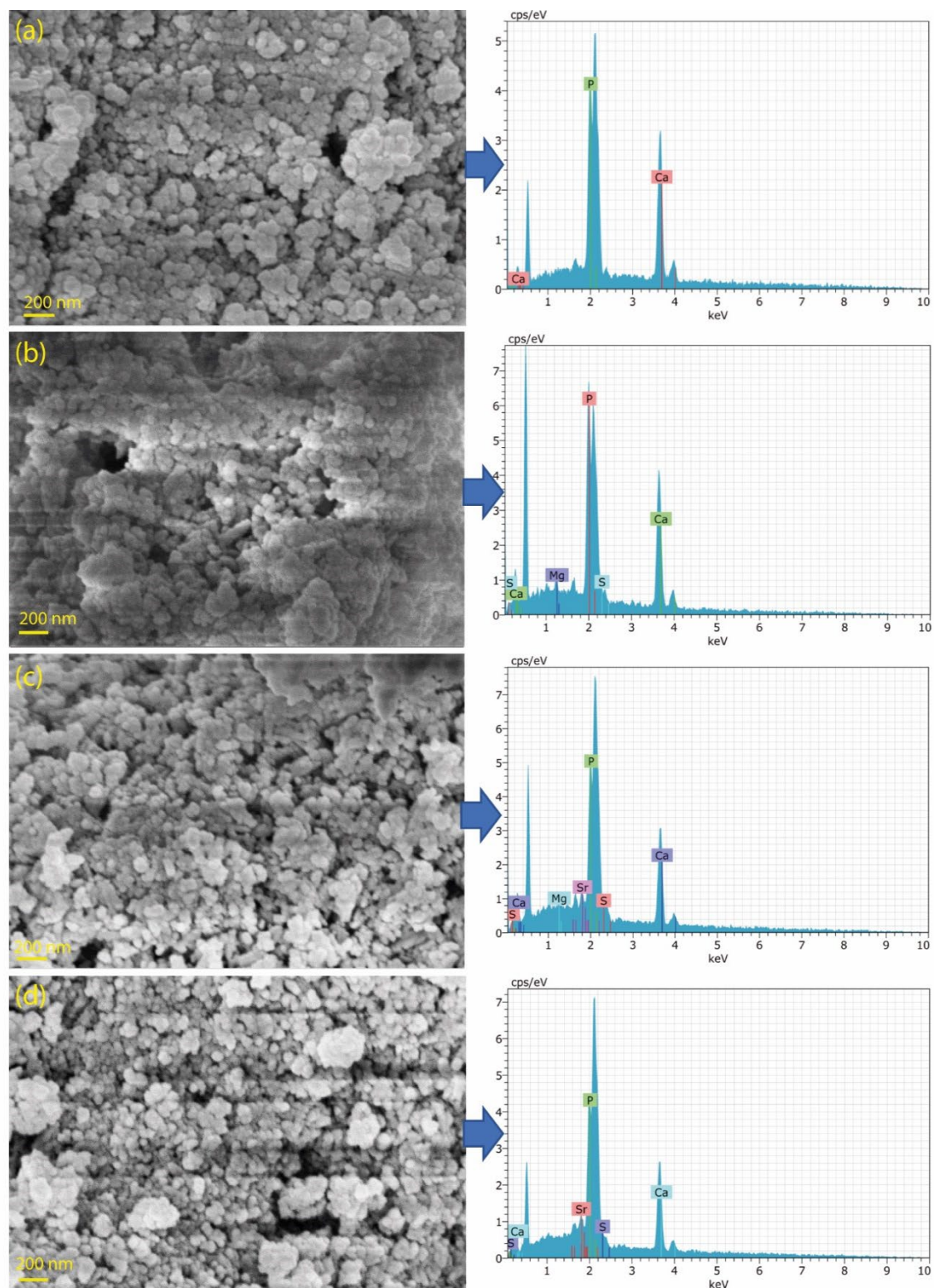


Fig. 5. FESEM images of (a) pure HA, (b) 1Mg-SHA, (c) 4MgSr-SHA, and (g) 6Sr-SHA calcined at 500 °C.

To compare the atomic composition of HA and Mg Sr-SHA nanoparticles, see Table 3. In contrast to what was predicted (1.67), the Ca/P ratio of HA nanoparticles was only 1.59. The substitution of Mg and Sr ions for Ca resulted in a fall in Ca's atomic percentage, bringing this ratio down to 0.97-1.20 for MgSr-SHA samples. Because of the changes in atomic contacts and the ensuing local organization, the capacity of atoms to construct an ordered crystalline structure at

the outer surface of nanoparticles during the calcination process may be distorted, leading to the development of an amorphous surface phase. Additionally, the cooling process proceeded more rapidly at the surface layer than in the core of the nanoparticles, leaving insufficient time for atoms to adopt a crystalline spatial arrangement.

Table 3. Pure HA and MgSr-SHA series chemical composition.

| Sample ID | Chemical Compositions (Mass (%)) | | | | | Ca+Mg+Sr/P+S atomic ratios | |
|-----------|----------------------------------|-------|------|------|------|----------------------------|--------------|
| | Ca | P | S | Mg | Sr | Theoretical | Experimental |
| HA | 67.33 | 32.67 | 00 | 00 | 00 | 1.67 | 1.59 |
| 1Mg-SHA | 57.16 | 39.21 | 3.10 | 0.53 | 00 | 1.67 | 1.06 |
| 4MgSr-SHA | 51.38 | 39.68 | 3.70 | 0.44 | 4.80 | 1.67 | 0.97 |
| 6Sr-SHA | 55.86 | 34.99 | 3.01 | 00 | 6.15 | 1.67 | 1.20 |

4. Conclusions

In summary, monophasic HA substituted by Mg²⁺ and Sr²⁺ cation and SO₄²⁻ anion was successfully obtained using microwave irradiation-assisted wet-precipitation technique. The incorporation of Mg²⁺, Sr²⁺, and SO₄²⁻ ions resulted in a reduction in crystallinity, validated by XRD and FTIR spectroscopy. The results suggested that the incorporation of the ions caused this drop. XRD results also showed fluctuation in the lattice parameters and a reduction in crystallite size. The incorporation of a high amount of Sr ions increased the thermal stability of the Mg-SHA materials. FTIR result indicated broadening in the phosphate band and disappearance of bending vibration of OH group, which is the effect of SO₄ group replacement to maintain the charge of HA in balance. The dopants have no impact on the morphology of particles. The Ca/P ratios of the prepared materials were lower than the theoretical value.

Acknowledgements

Dr. Ammar Z. Alshemary would like to thank Karabuk University for providing financial support via Project no. KBÜBAP-22-DS-007. Dr. Ammar Z. Alshemary would like to thank Al-Mustaqbal University College.

References

- [1] M.O. Li, X. Xiao, R. Liu, C. Chen, L. Huang, *Journal of Materials Science: Materials in Medicine*, 19, 797-803(2008); <https://doi.org/10.1007/s10856-007-3213-4>
- [2] S. Kannan, J.M.G. Ventura, J.M.F. Ferreira, *Ceramics International*, 33, 1489-1494(2007); <https://doi.org/10.1016/j.ceramint.2006.05.016>
- [3] A.Z. Alshemary, Y.-F. Goh, M. Akram, I.R. Razali, M.R. Abdul Kadir, R. Hussain, *Materials Research Bulletin*, 48, 2106-2110(2013); <https://doi.org/10.1016/j.materresbull.2013.02.015>
- [4] J.G. Aqif Anwar Chaudhry, Martin Vickers, Jeremy Karl Cockcroft, Ihtesham Rehman, Jonathan Knowles and Jawwad Arshad Darr, *Journal of Materials Chemistry*, 18, 5900-5908 (2008); <https://doi.org/10.1039/b807920j>
- [5] S.M.B.a.W.B. N. Patel, *J. Aust. Ceram. Soc.* 41[2], 1-22, (2005).
- [6] E. Shorr, A.C. Carter, *Bulletin of the Hospital for Joint Diseases*, 13, 59-66(1952).
- [7] P.J. Marie, *Osteoporosis International*, 16, S7-S10 (2005); <https://doi.org/10.1007/s00198-004-1753-8>
- [8] P. Ammann, *Osteoporosis International*, 16, S11-S15(2005); <https://doi.org/10.1007/s00198->

[004-1809-9](#)

- [9] W.L. Suchanek, K. Byrappa, P. Shuk, R.E. Riman, V.F. Janas, K.S. Tenhuisen, *Biomaterials*, 25, 4647-4657(2004); <https://doi.org/10.1016/j.biomaterials.2003.12.008>
- [10] P.M. Cerrato, *J.Registered Nurses*, 61, 57-58(1998).
- [11] N.D. Gregory S. Kelly, *Alternative Medicine Review*, 3(1), 27-39(1998).
- [12] A.M. Castillo-Paz, S.M. Londoño-Restrepo, L. Tirado-Mejía, M.A. Mondragón, M.E. Rodríguez-García, *Progress in Natural Science: Materials International*, 30, 494-501(2020); <https://doi.org/10.1016/j.pnsc.2020.06.005>
- [13] E. Landi, S. Guizzardi, E. Papa, C. Galli, *Applied Sciences*, 11, 4930(2021); <https://doi.org/10.3390/app11114930>
- [14] X. Hu, H. Shen, K. Shuai, E. Zhang, Y. Bai, Y. Cheng, X. Xiong, S. Wang, J. Fang, S. Wei, *Applied Surface Science*, 257, 1813-1823 (2011). <https://doi.org/10.1016/j.apsusc.2010.08.082>